



pH monitoring in high ionic concentration environments: performance study of graphene-based sensors

Xin Qi¹ · Wei Jin¹ · Cao Tang¹ · Xue Xiao¹ · Rui Li¹ · Yanqing Ma^{1,2,3} · Lei Ma^{1,2} 

Received: 22 July 2024 / Accepted: 15 October 2024

© The Author(s), under exclusive licence to The Japan Society for Analytical Chemistry 2024

Abstract

Graphene-based pH sensors, acclaimed for their exceptional sensitivity to environmental variations, have garnered significant interest in scientific research. However, the sensor performance in high ionic concentration environments is limited, due to the Debye length ion screening effect. In this study, an innovative graphene channel pH sensing device was developed and modified by cross-linked poly(methyl methacrylate) (PMMA). Furthermore, even in high ionic concentrations, the pH value can be precisely measured by this sensor. The sensor has remarkable sensitivity, and high response rate of -70.49 mV/pH within the pH range from 7 to 10. Notably, the sensors retain uniform response direction and sensitivity under different ionic concentrations environmental and maintain consistent reversibility and stability. This advancement in sensor technology paves the way for broader applications in complex ionic environments.

Keywords CVD graphene · pH sensor · High ionic concentration · Solution gate field-effect transistor

Introduction

The pivotal role of pH measurement in diverse domains, such as environmental monitoring, industrial processes, and biomedical applications, is indisputable. It forms an essential foundation for the effective functioning of these systems [1]. In the context of the increasing integration of sensors into everyday life, there is a growing demand for their portability and miniaturization. This evolution has revealed the limitations of traditional pH sensors, including glass electrodes, optical [2, 3], and acoustic types [4], which are becoming progressively impractical for modern applications. In recent

years, the application of graphene-based field-effect transistors (GFETs) in the field of sensing has effectively filled a significant gap in this domain [5–15]. The unique attribute of graphene, being just a single atomic layer thick, endows it with exceptional electrical sensitivity to environmental changes. This sensitivity, combined with its inherent suitability for miniaturization, significantly enhances the portability of these sensors.

In 2008, Ang [16] innovatively proposed the use of graphene-based liquid gate field-effect transistors for pH measurement. Utilizing epitaxial graphene as the channel material, this approach achieved a remarkable sensitivity up to 99 mV/pH. Building on this foundational work, in 2015, Lee et al. [17] reported a sensitivity of -59 mV/pH in pH response tests conducted in a 0.05 M phosphate buffer solution, within a pH range from 6 to 8. Interestingly, altering the electrolyte to a 0.005 M phosphate buffer solution modulated the sensitivity to 50 mV/pH in the same pH range. The sensitivity of sensors is significantly influenced by the concentration of ions. Further advancing the field, Jung et al. [18] further advanced the field by engineering a highly sensitive pH sensor with a negative V_{dir} response. This was accomplished through defect engineering in nano-crystalline graphene, characterized by numerous grain boundaries, and leveraging proton charge transfer doping, culminating in an impressive sensitivity of -140 mV/pH.

✉ Yanqing Ma
mayanqing@tju.edu.cn

✉ Lei Ma
lei.ma@tju.edu.cn

¹ Tianjin International Center for Nanoparticles and Nanosystems, Tianjin University, 92 Weijin Road, Nankai District, Tianjin 300072, People's Republic of China

² Tianjin Key Laboratory of Low-Dimensional Electronic Materials and Advanced Instrumentation, Tianjin 300072, People's Republic of China

³ School of Precision Instrument and Opto-Electronic Engineering, Tianjin University, Tianjin 300072, People's Republic of China

At ambient temperature, the Debye length for a 100 mM electrolyte solution is approximately 1.3 nm [19]. Beyond this Debye length, the charges present in the solution cease to affect the channel potential, which presents a significant challenge for pH detection. Currently, graphene-based pH sensors are predominantly evaluated in phosphate-buffered saline (PBS) solutions with concentrations ranging from 2 to 50 mM [16, 20–26]. However, in many biological environments, ion concentrations often surpass 100 mM. For instance, the osmotic concentration in extracellular fluid and human serum typically lies between 277 and 305 mOsmol/Kg. This translates to ion concentrations approximately ranging from 270 to 297.4 mM [27]. Such high ion concentrations necessitate desalting processes when testing human body fluids, underscoring the critical need for expanding the applicability of pH testing in environments with high ionic concentrations.

Our research utilized reactive ion etching to pattern graphene synthesized via chemical vapor deposition (CVD). Then, the graphene channel attached to a cross-linked PMMA film is fabricated as an innovative pH sensor. This sensor was rigorously tested in a 1×PBS buffer solution, where the neutrality point voltage (V_{dir}) consistently shifted negatively with increasing pH levels (6.81–10.12), showing a sensitivity of -67.76 mV/pH. In a high-concentration 10×PBS buffer solution (100 mM phosphate), the sensor maintained a sensitivity of -70.49 mV/pH without changing the response direction. This study demonstrates a pH sensor that operates effectively in high ionic concentrations with minimal sensitivity fluctuations.

Experimental section

Growth and characterization of graphene

Graphene films were synthesized utilizing the chemical vapor deposition (CVD) technique, with methane serving as the precursor, on copper foil with a thickness of 25 μ m. The detailed synthesis process is outlined as follows: initially, the copper foil, subjected to thorough cleaning, was positioned inside a quartz tube. This assembly was subsequently heated in a tubular furnace (model GSL-1700X-III, manufactured by Hefei Kejing Material Technology Co., Ltd.) from ambient temperature to 1078 °C at a controlled rate of 9 °C/min. The argon gas flow was meticulously regulated at 200 sccm. Upon attaining the target temperature, a mixture of hydrogen and argon gasses (in a flow ratio of 1:10) was introduced and sustained for a duration of 60 min. Following this, methane was injected at a flow rate of 1 sccm, with the growth period precisely timed to 10.5 min. Post-growth, the sample was methodically cooled in a hydrogen–argon (H_2/Ar) atmosphere.

To evaluate the quality of the synthesized graphene, a Raman spectrometer (model RTS-2, equipped with an Andor 500 spectrometer) was employed.

Fabrication, characterization, and testing of graphene field-effect transistor devices

Figure 1 delineates the comprehensive fabrication process of the graphene field-effect transistor device. The process commenced with the utilization of photolithography (Micro-lab 4A-100, Suzhou Suda Vigo Optoelectronics Technology Co., Ltd.) and electron beam evaporation (PS-3, Chengdu Xingnan Technology Co., Ltd.) to create 20 nm chromium (Cr)/20 nm gold (Au) electrodes on a silicon/silicon dioxide (Si/SiO₂) substrate, featuring a 285 nm oxide layer.

A layer of PMMA (495A4, MicroChem) was spin-coated onto the surface of graphene pre-grown on copper foil at a speed of 4000 rpm. The copper/graphene/PMMA assembly was then immersed in a potassium persulfate solution until the copper foil was completely dissolved. Afterward, the graphene with the PMMA layer was transferred onto a silicon wafer equipped with electrodes.

Subsequently, the sample was immersed in acetone to remove most of the PMMA, although some residues remained on the graphene surface. The next step was to pattern the graphene. Specifically, the graphene and the residual PMMA layer were covered with S1813 photoresist, followed by reactive ion etching (RIE-150, Theron Technology Co., Ltd.) with oxygen plasma for 15 s. The oxygen flow rate was 50 sccm, and the power was set to 35 watts, which allowed for precise removal of graphene outside the channel areas. During this patterning process, the PMMA on the graphene surface in the channel regions underwent cross-linking due to the energy generated through this etching process. Subsequently, the photoresist mask was dissolved in acetone, exposing the graphene/cross-linked PMMA layer.

The final step involves applying S1813 photoresist for encapsulation. After spin-coating the photoresist onto the sample, the graphene channel, gate, and electrode pad areas are exposed using ultraviolet light at a wavelength of 405 nm. Following development with a sodium hydroxide solution, the exposure of the aforementioned areas is completed.

For morphological characterization of the samples, an atomic force microscope (AFM, NX-10, Park) and a scanning electron microscope (SEM, SU-3500, HITACHI) were employed. The chemical composition of the sample surface was analyzed using X-ray photoelectron spectroscopy (XPS, PHI 5100, Perkin Elmer).

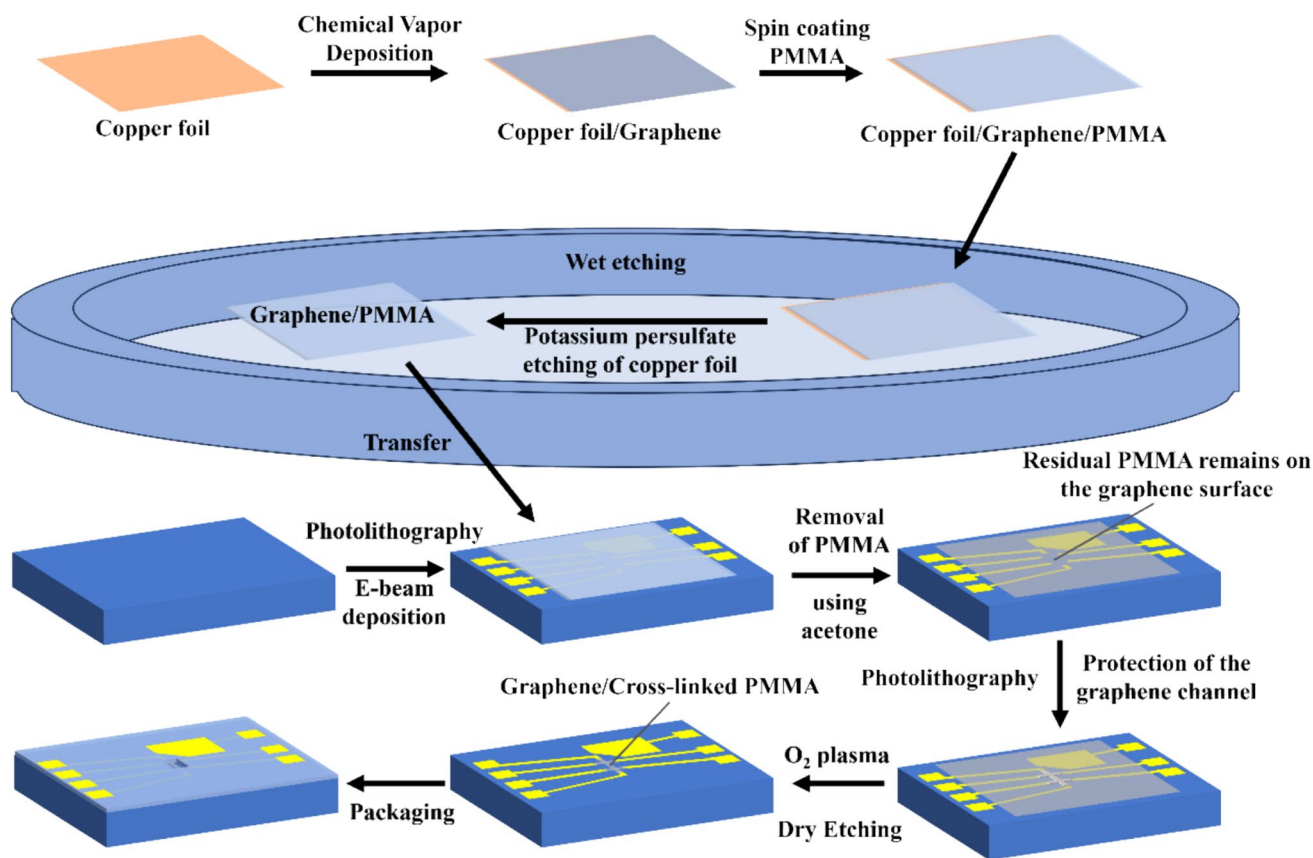


Fig. 1 Fabrication process diagram of the graphene field-effect transistor device

Preparation of pH solutions

In the experimental setup, buffer solutions were prepared using both $10\times$ PBS and a tenfold diluted $1\times$ PBS. The $10\times$ PBS solution contains 26.8 mM KCl, 20 mM KH_2PO_4 , 1.37 M NaCl, and 100 mM Na_2HPO_4 . To achieve a range of pH values, these solutions were systematically adjusted using small quantities of 0.5 M hydrochloric acid (HCl) and 0.5 M sodium hydroxide (NaOH).

Testing of pH sensing performance

Electrical signal testing was conducted using a probe station (Qianye, C-4) and a source meter (Keithley, 2600BS). As shown in Fig. 2a, Channel A of the source meter is connected to the source and drain; Channel B is connected to the gate and source. A 1–2 μL aliquot of the prepared pH solution was applied using a pipette (Dragonlab), ensuring the droplet covered the graphene channel and the entire gate area during testing.

Results and discussion

Device characterization

Figure 2a illustrates a schematic and circuit diagram of the liquid-gated graphene crystal transistor. Figure 2b shows the SEM image of the graphene channel in the sensor device. The image reveals that the CVD graphene transferred onto the device is etched into a HallBar shape. Figure 2c clearly shows the etched boundaries of the graphene channel and a layer of cross-linked PMMA film covering the graphene surface, formed after ion bombardment for graphene patterning. The height image reveals that the thickness of the graphene and the film is approximately 10.14 nm. Figure 2d presents the Raman spectrum of the graphene channel, with peaks at 1340 cm^{-1} , 1588 cm^{-1} , and 2681 cm^{-1} corresponding to the D, G, and 2D characteristic peaks of graphene, respectively. The D peak, indicative of graphene's defects, arises from phonon intervalley scattering due to defects and amorphous regions. The G peak originates from the in-plane vibration of sp^2 hybridized carbon atoms, a doubly degenerate (TO and LO) phonon mode at the center of the Brillouin

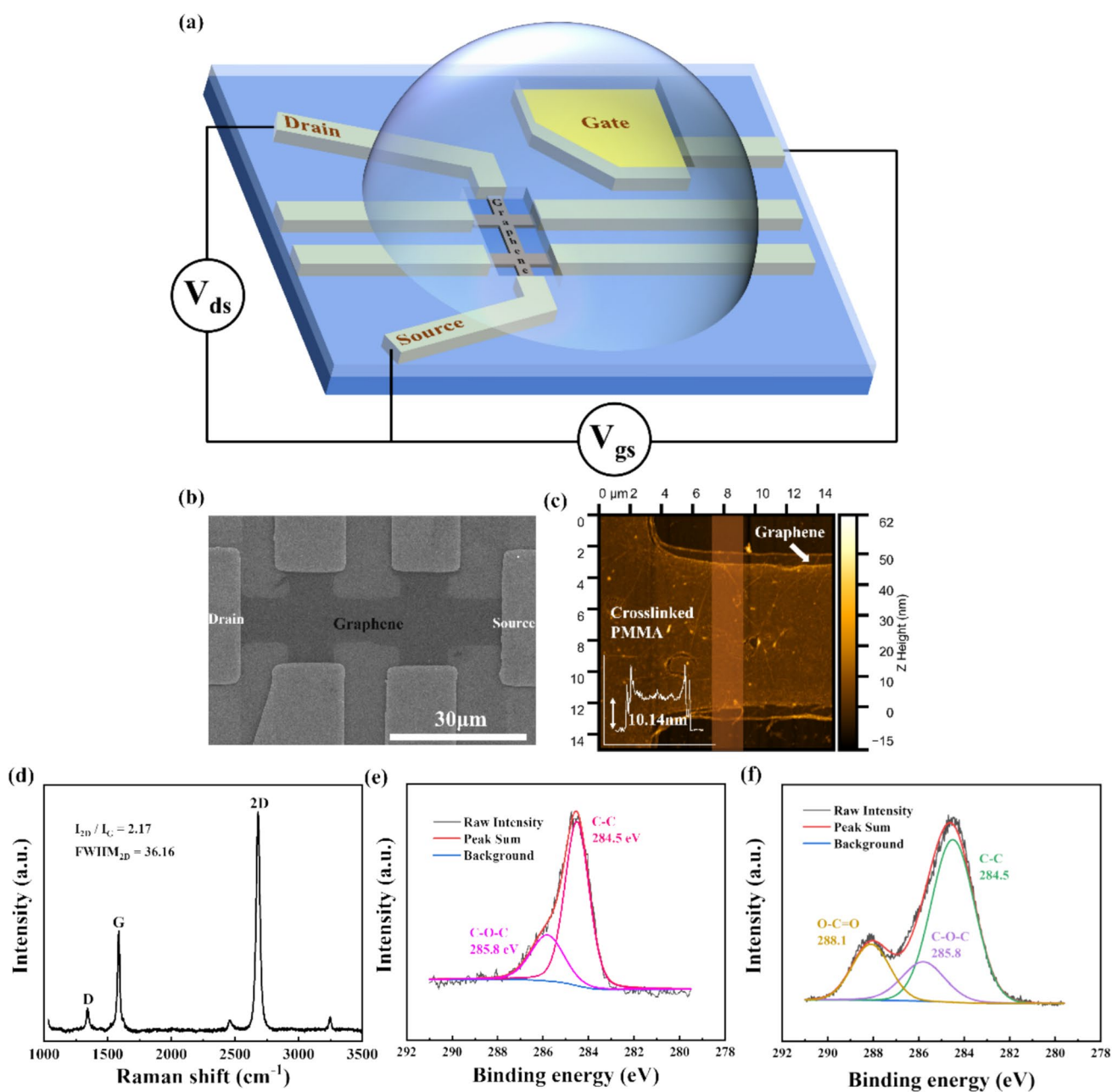


Fig. 2 **a** Schematic diagram of the graphene field-effect transistor pH sensor; **b** scanning electron microscope image of the graphene channel; **c** atomic force microscope image of the field-effect transistor graphene channel; **d** Raman spectrum of CVD graphene; **e** C1s core

level peak in the X-ray photoelectron spectroscopy spectrum of the graphene channel; **f** C1s core level peak in the XPS spectrum of polymethyl methacrylate (PMMA)

zone, reflecting graphene's lattice structure and symmetry. The 2D peak results from the electron's double resonance scattering process, closely related to the band structure of graphene layers and sensitive to the number of layers and stacking method [28–32]. The full width at half-maxima of the 2D peak in the Fig. 2d is 36.16 cm^{-1} , and the intensity ratio of the 2D and G peaks (I_{2D}/I_G) is 2.17, indicating the material is monolayer graphene [22, 33]. An atomic force

microscope scan of the graphene channel was conducted. The cross-linked PMMA film was characterized by XPS as shown in Fig. 2e. Following high-energy ion beam irradiation, the XPS analysis of the etched PMMA shows a near absence of the carboxyl carbon peak (288.1 eV) compared to the initial PMMA as depicted in Fig. 2f. This indicates a significant reduction in the carboxyl groups within the PMMA after irradiation. Highly polar carboxyl groups were

diminished after reduction [34]. This observation aligns with our findings that cross-linked PMMA films are insoluble in organic solvents. Under the influence of high-energy radiation, chemical bonds in PMMA are disrupted, leading to the formation of free radicals. The reduction of carboxyl groups increases the degree of unsaturation [35], potentially leading to the formation of new free radicals from unpaired carbon atoms. These free radicals act as potential active centers for cross-linking reactions. These free radicals react with unsaturated carbon atoms, facilitating the formation of carbon–carbon cross-links. This process increases the cross-link density of the material, thereby enhancing its overall stability [36].

Sensor performance testing

Figure 3a shows source–drain current versus gate voltage curves for the graphene-based pH sensor, measured at a source–drain voltage (V_{ds}) of 0.1 V, while the gate voltage was scanned between 0.4 and 1.4 V in 1 × PBS of various pH values. Graphene-based pH sensor exhibited ambipolar behaviors. Graphene's electronic band structure includes a unique point known as the neutrality point, at which the energies of electrons and holes are equal, resulting in zero electron density. The application of varying gate voltages modifies the Fermi level in graphene. On the left side of the neutrality point, holes are the primary charge carriers; as the gate voltage increases, the Fermi level shifts upward, reducing the hole concentration and causing a decrease in current. Conversely, on the right side of the neutrality point, electrons become the primary charge carriers; with increasing gate voltage, the electron concentration rises, leading

to an increase in current. This phenomenon underlies the bipolar behavior observed in the transfer characteristic curve [37, 38].

Notably, in the environment of the PBS buffer solution, V_{dir} registered positive values, indicating the presence of p-type doping in graphene [39]. This doping phenomenon is attributed to a combination of factors: the interaction with water and oxygen molecules from the ambient air, and the coverage by the cross-linked PMMA film. Given that PMMA is an electron-withdrawing material, it effectively withdraws electrons from the graphene, resulting in pronounced p-type doping characteristics [40]. As illustrated in Fig. 3b, when the electrolyte pH increases from 6.81 to 10.12, the transfer characteristic curve shifts toward the negative direction, with the charge neutrality point shifting from 1.19 to 0.94, demonstrating a sensitivity of -67.76 mV/pH.

As the pH increases, the phenomenon of a negative shift in the neutrality point voltage is uncommon. This negative pH response does not align with the traditional electrostatic model, which posits that the shift of the charge neutrality point is influenced by the electrostatic gating of the double electric layer formed on the graphene interface, typically resulting in a positive shift of V_{Dir} with increasing pH. However, this can be analyzed from the perspective of charge doping. Previous studies have discussed the reversible hydrogenation of graphene devices when immersed in hydrogen ion-containing solutions under an electric field [41]. During the reaction between graphene and hydrogen ions, the hydrogen ions transfer their protons to a carbon atom in the graphene, leading to protonation and the formation of a C–H chemical bond. This reaction results in the loss of an electron from a carbon atom in the graphene,

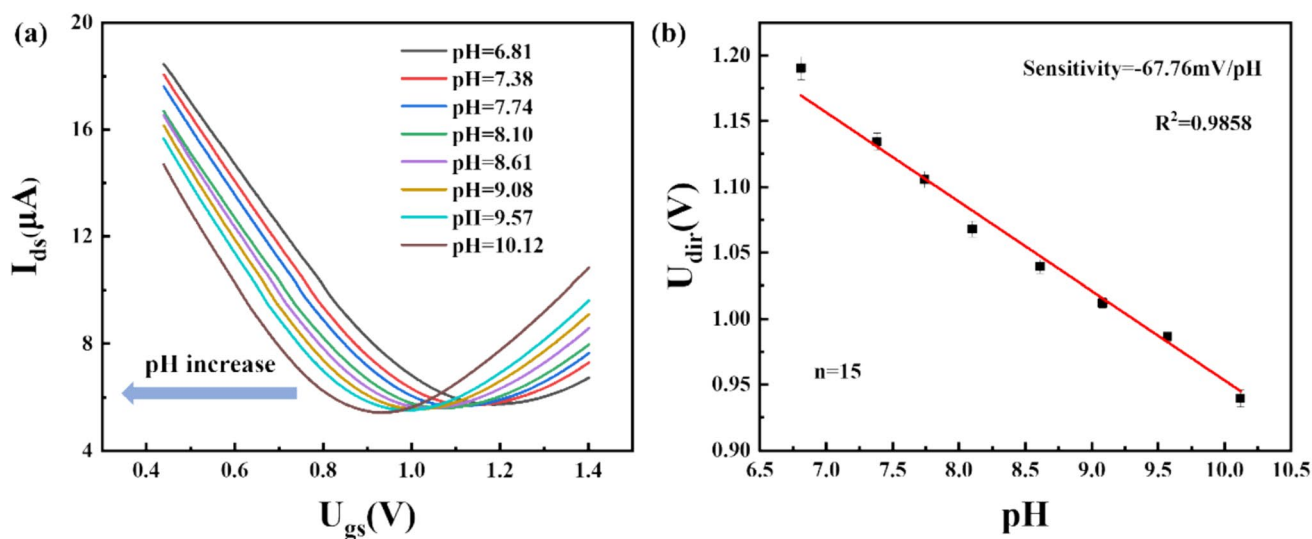


Fig. 3 **a** Transfer characteristic curves of the graphene-based pH sensor in different pH buffer solutions ranging from 6.81 to 10.12 in a 1 × PBS environment; **b** shift of neutrality point gate voltage in different pH solutions

thereby increasing the hole concentration and shifting the transfer characteristic curve in the positive direction. This mechanism can explain the observed negative shift in V_{Dir} with increasing pH.

The cross-linked PMMA film on the graphene surface suppresses the influence of the electrostatic model, highlighting the effect of proton doping. Jung [18] has discussed pH sensors based on the charge doping mechanism and experimentally demonstrated that sensors utilizing direct charge transfer doping effects exhibit higher pH sensitivity.

To evaluate the sensitivity of this sensor more directly, we compared it with other graphene-based pH sensors that have been reported. As shown in Fig. 4, the graphene-based pH sensor developed in this study achieves a sensitivity of

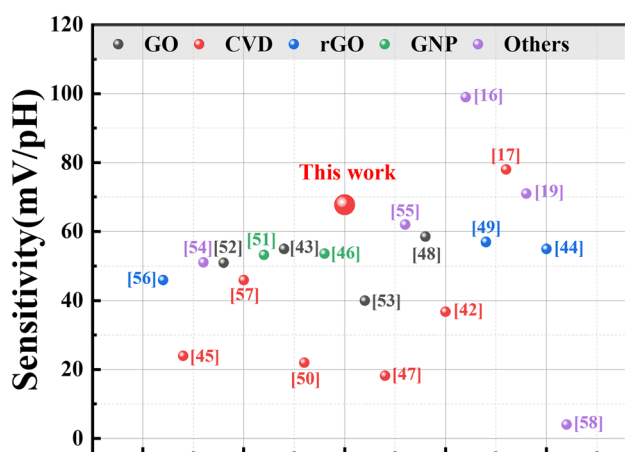


Fig. 4 Sensitivity comparison of different graphene-based pH sensors [16, 17, 19, 42–58]

67.76 mV/pH, surpassing most of the pH sensors reported previously.

To test whether our graphene-based pH sensor can resist the effects caused by an increase in ion concentration in the external liquid environment, the electrolyte solution was replaced with $10\times$ PBS, which has a tenfold increase in ion concentration. Testing was conducted within a pH range of 6.78 to 10.06. As shown in Fig. 5b, when the pH of the electrolyte increased from 6.78 to 10.06, the transfer characteristic curve continued to shift in the negative direction, with V_{Dir} gradually shifting by 0.24 V, demonstrating a sensitivity of -70.49 mV/pH.

As shown in Fig. 6a, comparing the results tested in $1\times$ and $10\times$ PBS environments, it is observed that the direction of V_{dir} shift remains unchanged in high electrolyte concentration tests compared to those in lower electrolyte environments. The sensitivity fluctuates within 4%, which is significantly lower compared to previous reports where a tenfold increase in electrolyte concentration led to a change in the direction of V_{dir} shift and a 218% change in sensitivity. The devices fabricated in this study show minimal influence from surrounding electrolyte concentrations. According to Koval's research, cross-linked PMMA films swell when immersed in acetone [59].

Figure 6b displays results from five consecutive tests in a $10\times$ PBS environment, showing concentrated data points with similar shift directions and close sensitivities (approximately 5 mV/pH fluctuation), indicating good repeatability and stability of the devices.

Further, reverse pH gradient tests were conducted on the fabricated pH sensor devices, where the electrolyte pH was gradually decreased from 10.06 to 6.78. As shown in Fig. 6c,

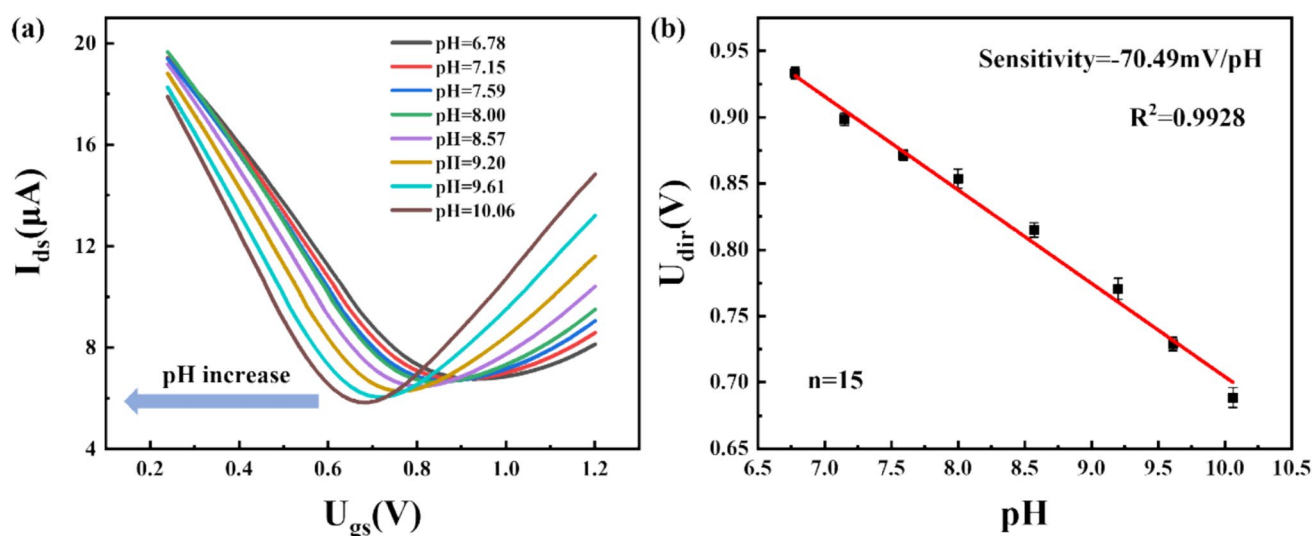


Fig. 5 **a** Transfer characteristic curves of the graphene-based pH sensor in different pH buffer solutions ranging from 6.78 to 10.06 in a $10\times$ PBS environment; **b** shift of neutrality point gate voltage in different pH solutions

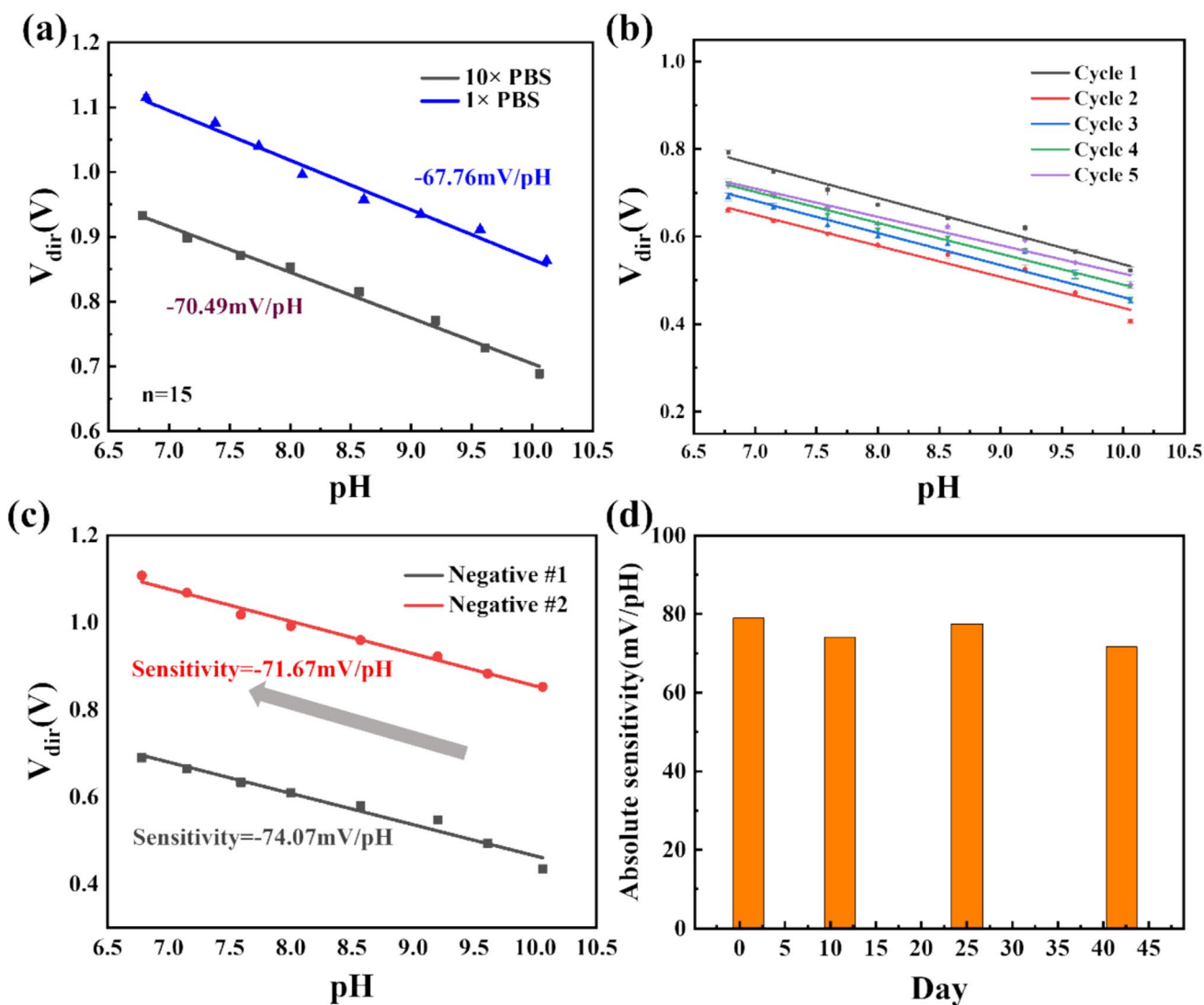


Fig. 6 **a** Sensitivity comparison of graphene-based sensors to pH under different electrolyte concentrations; 10×PBS (black) and 1×PBS (blue); **b** correspondence graph of V_{Dir} and pH across five consecutive test cycles of a graphene field-effect transistor; **c** corre-

spondence graph of V_{Dir} and pH for reverse pH gradient tests on two graphene field-effect transistor sensors from the same batch; **d** graph showing the change in device sensitivity over time

the sensitivities of the two devices were -71.67 mV/pH and -74.07 mV/pH , respectively, similar to the forward gradient test sensitivity of -70.49 mV/pH , thereby demonstrating the reversibility of the pH response for graphene-based sensor. Additionally, after the device was stabilized, pH tests were conducted on the 1st, 11th, 25th, and 42nd day, and the sensitivities were statistically analyzed as shown in Fig. 6d. The sensitivity of device was well-maintained over this period. However, as observed in Figs. 6a and S2, despite the unchanged sensitivity, there was a general vertical shift in the distribution of V_{dir} over time. In contrast, when the field-effect transistor was used for consecutive short-term transfer characteristic tests in 10× and 1× electrolytes, no significant shift occurred as shown in Figure S3.

We propose that the pore structure of the swollen cross-linked PMMA obstructs the passage of larger sodium and potassium ions, while relatively smaller hydrogen ions can conduct in the aqueous phase, as shown in Fig. 7. This is the reason of changing the electrolyte ion concentration does not significantly alter the sensitivity.

For $\text{pH} < 6$, and it was found that regardless of whether 10×PBS or 1×PBS was used as the electrolyte, the neutrality point shifted positively with increasing pH, as shown in Figure S4. In a 10×PBS environment, the data distribution is more linear, with a sensitivity of approximately 120.14 mV/pH . The sensor maintains a high sensitivity of 133.99 mV/pH within the pH range of approximately 3.5–4.5, but near pH 4.5–6, the neutrality point shows almost

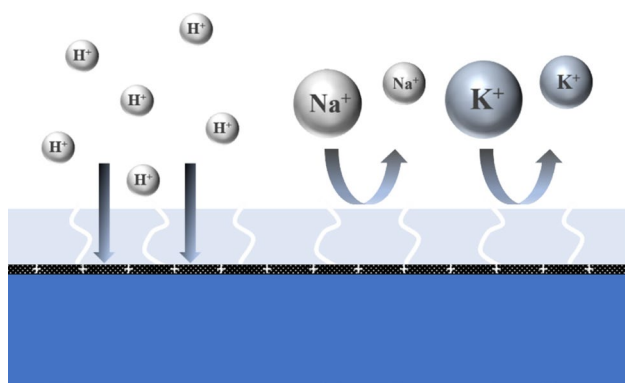


Fig. 7 Mechanism diagram of shielding the effects of ion concentration changes in liquid environments

no change with varying pH. Further optimization is needed to expand the application range of sensor.

Conclusion

In this paper, we successfully implemented cross-linked PMMA onto graphene surfaces to achieve pH measurement in high ionic concentration environments. The cross-linked PMMA was formed by bombarding the PMMA layer with high-energy ion beams during the graphene patterning process. The graphene-based pH sensor fabricated using this method showed high sensitivity of approximately -67.76 mV/pH in low ionic concentration environments within a pH range from 6.81 to 10.12. Moreover, when the ionic concentration was increased tenfold, both response direction and sensitivity remained largely unchanged, demonstrating its viability in high ionic concentration environments. The inverse concentration gradient tests also indicated good reversibility of the sensor. Additionally, stability tests revealed that the sensitivity remained consistent over a period of 42 days.

Overall, this study presents an effective method of enhancing graphene-based pH sensor, successfully addressing the challenges in high ionic concentration environments. The sensor not only exhibits high sensitivity, good reversibility, and stability but also maintains consistent performance amidst varying ionic concentrations, suggesting a broad spectrum of potential applications.

Supplementary Information The online version contains supplementary material available at <https://doi.org/10.1007/s44211-024-00682-9>.

Acknowledgements This work was financially supported by the National Key R&D Program of China (No. 2022YFC3006303)

Data availability The availability of Data and Materials are manuscript and Supplementary materials.

References

1. M.I. Khan, K. Mukherjee, R. Shoukat et al., A review on pH sensitive materials for sensors and detection methods. *Microsyst. Technol.* **23**, 4391–4404 (2017)
2. B. Lakard, G. Herlem, M. de Labachellerie et al., Miniaturized pH biosensors based on electrochemically modified electrodes with biocompatible polymers. *Biosens. Bioelectron.* **19**(6), 595–606 (2004)
3. M. Yuqing, C. Jianrong, F. Keming, New technology for the detection of pH. *J. Biochem. Biophys. Methods* **63**(1), 1–9 (2005)
4. H.-F. Ji, K. Hansen, Z. Hu et al., Detection of pH variation using modified microcantilever sensors. *Sens. Actuators B Chem.* **72**(3), 233–238 (2001)
5. S.K. Ameri, P. Singh, S. Sonkusale, Utilization of graphene electrode in transparent microwell arrays for high throughput cell trapping and lysis. *Biosens. Bioelectron.* **61**, 625–630 (2014)
6. L.H. Hess, M. Jansen, V. Maybeck et al., Graphene transistor arrays for recording action potentials from electrogenic cells. *Adv. Mater.* **23**(43), 5045–5049 (2011)
7. Y. Shao, J. Wang, H. Wu et al., Graphene based electrochemical sensors and biosensors: a review. *Electroanalysis* **22**(10), 1027–1036 (2010)
8. Y. Wu, K.A. Jenkins, A. Valdes-Garcia et al., State-of-the-art graphene high-frequency electronics. *Nano Lett.* **12**(6), 3062–3067 (2012)
9. Y. Wu, Y.-M. Lin, A.A. Bol et al., High-frequency, scaled graphene transistors on diamond-like carbon. *Nature* **472**(7341), 74–78 (2011)
10. Y. Zhang, Y.-W. Tan, H.L. Stormer et al., Experimental observation of the quantum Hall effect and Berry's phase in graphene. *Nature* **438**(7065), 201–204 (2005)
11. T.H. Han, Y.-K. Huang, A.T. Tan et al., Steam etched porous graphene oxide network for chemical sensing. *J. Am. Chem. Soc.* **133**(39), 15264–15267 (2011)
12. Y. Huang, X. Dong, Y. Liu et al., Graphene-based biosensors for detection of bacteria and their metabolic activities. *J. Mater. Chem.* **21**(33), 12358–12362 (2011)
13. M. Pumera, Graphene in biosensing. *Mater. Today* **14**(7–8), 308–315 (2011)
14. H.G. Sudibya, Q. He, H. Zhang et al., Electrical detection of metal ions using field-effect transistors based on micropatterned reduced graphene oxide films. *ACS Nano* **5**(3), 1990–1994 (2011)
15. S. Zhang, D. Zhang, V.I. Sysoev et al., Wrinkled reduced graphene oxide nanosheets for highly sensitive and easy recoverable NH₃ gas detector. *RSC Adv.* **4**(87), 46930–46933 (2014)
16. P.K. Ang, W. Chen, A.T.S. Wee et al., Solution-gated epitaxial graphene as pH sensor. *J. Am. Chem. Soc.* **130**(44), 14392–14393 (2008)
17. M.H. Lee, B.J. Kim, K.H. Lee et al., Apparent pH sensitivity of solution-gated graphene transistors. *Nanoscale* **7**(17), 7540–7544 (2015)
18. S.-H. Jung, Y.-M. Seo, T. Gu et al., Super-Nernstian pH sensor based on anomalous charge transfer doping of defect-engineered graphene. *Nano Lett.* **21**(1), 34–42 (2020)
19. S.K. Ameri, P.K. Singh, S.R. Sonkusale, Three dimensional graphene transistor for ultra-sensitive pH sensing directly in biological media. *Anal. Chim. Acta* **934**, 212–217 (2016)
20. Z. Cheng, Q. Li, Z. Li et al., Suspended graphene sensors with improved signal and reduced noise. *Nano Lett.* **10**(5), 1864–1868 (2010)
21. W. Fu, C. Nef, O. Knopfmacher et al., Graphene transistors are insensitive to pH changes in solution. *Nano Lett.* **11**(9), 3597–3600 (2011)

22. B. Maily-Giacchetti, A. Hsu, H. Wang et al., pH sensing properties of graphene solution-gated field-effect transistors. *J. Appl. Phys.* **114**(8), 084505 (2013)
23. Y. Ohno, K. Maehashi, Y. Yamashiro et al., Electrolyte-gated graphene field-effect transistors for detecting pH and protein adsorption. *Nano Lett.* **9**(9), 3318–3322 (2009)
24. J. Ristein, W. Zhang, F. Speck et al., Characteristics of solution gated field effect transistors on the basis of epitaxial graphene on silicon carbide. *J. Phys. D Appl. Phys.* **43**(34), 345303 (2010)
25. X. Tan, H.-J. Chuang, M.-W. Lin et al., Edge effects on the pH response of graphene nanoribbon field effect transistors. *J. Phys. Chem. C* **117**(51), 27155–27160 (2013)
26. A. Lampinen, E. See, A. Emelianov et al., Laser-induced tuning of graphene field-effect transistors for pH sensing. *Phys. Chem. Chem. Phys.* **25**(15), 10778–10784 (2023)
27. C. Waymouth, Osmolality of mammalian blood and of media for culture of mammalian cells. *In Vitro* **6**(2), 109–127 (1970)
28. I. Calizo, A.A. Balandin, W. Bao et al., Temperature dependence of the Raman spectra of graphene and graphene multilayers. *Nano Lett.* **7**(9), 2645–2649 (2007)
29. C. Casiraghi, A. Hartschuh, H. Qian et al., Raman spectroscopy of graphene edges. *Nano Lett.* **9**(4), 1433–1441 (2009)
30. Z. Ni, Y. Wang, T. Yu et al., Raman spectroscopy and imaging of graphene. *Nano Res.* **1**(4), 273–291 (2010)
31. Z.H. Ni, T. Yu, Y.H. Lu et al., Uniaxial strain on graphene: Raman spectroscopy study and band-gap opening. *ACS Nano* **2**(11), 2301–2305 (2008)
32. M.A. Pimenta, G. Dresselhaus, M.S. Dresselhaus et al., Studying disorder in graphite-based systems by Raman spectroscopy. *Phys. Chem. Chem. Phys.* **9**(11), 1276–1291 (2007)
33. L.G. Cançado, A. Reina, J. Kong et al., Geometrical approach for the study of G' band in the Raman spectrum of monolayer graphene, bilayer graphene, and bulk graphite. *Phys. Rev. B* (2008). <https://doi.org/10.1103/PhysRevB.77.245408>
34. A. Licciardello, M.E. Fragalà, G. Foti et al., Ion beam effects on the surface and on the bulk of thin films of polymethylmethacrylate. *Nucl. Instrum. Methods Phys. Res. Sect. B Beam Interact. Mater. Atoms* **116**(1–4), 168–172 (1996)
35. J.O. Choi, J.A. Moore, J.C. Corelli et al., Degradation of poly(methylmethacrylate) by deep ultraviolet, x-ray, electron beam, and proton beam irradiations. *J. Vac. Sci. Technol. B Microelectron. Process. Phenom.* **6**(6), 2286–2289 (1988)
36. Y. Gao, D. Zhou, J. Lyu et al., Complex polymer architectures through free-radical polymerization of multivinyl monomers. *Nat. Rev. Chem.* **4**(4), 194–212 (2020)
37. I. Heller, S. Chatoor, J. Männik et al., Influence of electrolyte composition on liquid-gated carbon nanotube and graphene transistors. *J. Am. Chem. Soc.* **132**(48), 17149–17156 (2010)
38. S.S. Kwon, J. Yi, W.W. Lee et al., Reversible and irreversible responses of defect-engineered graphene-based electrolyte-gated pH sensors. *ACS Appl. Mater. Interfaces* **8**(1), 834–839 (2016)
39. A. Beraud, M. Sauvage, C.M. Bazan et al., Graphene field-effect transistors as bioanalytical sensors: design, operation and performance. *Analyst* **146**(2), 403–428 (2021)
40. W. Choi, M.A. Shehzad, S. Park et al., Influence of removing PMMA residues on surface of CVD graphene using a contact-mode atomic force microscope. *RSC Adv.* **7**(12), 6943–6949 (2017)
41. S. Li, J. Li, Y. Wang et al., Large transport gap modulation in graphene via electric-field-controlled reversible hydrogenation. *Nat. Electron.* **4**(4), 254–260 (2021)
42. T.-E. Bae, H. Kim, J. Jung et al., Fabrication of high-performance graphene field-effect transistor with solution-processed Al₂O₃ sensing membrane. *Appl. Phys. Lett.* (2014). <https://doi.org/10.1063/1.4871865>
43. S. Chinnathambi, G.J.W. Euverink, Polyaniline functionalized electrochemically reduced graphene oxide chemiresistive sensor to monitor the pH in real time during microbial fermentations. *Sens. Actuators B Chem.* **264**, 38–44 (2018)
44. S. Chinnathambi, G.J.W. Euverink, Hydrothermally reduced graphene oxide as a sensing material for electrically transduced pH sensors. *J. Electroanal. Chem.* **895**, 115530 (2021)
45. J. Gao, Y. Wang, Y. Han et al., Graphene-based field-effect transistors integrated with microfluidic chip for real-time pH monitoring of seawater. *J. Mater. Sci. Mater. Electron.* **31**(18), 15372–15380 (2020)
46. D. Janczak, A. Peplowski, G. Wroblewski et al., Investigations of printed flexible pH sensing materials based on graphene platelets and submicron RuO₂ powders. *J. Sens.* **2017**, 1–6 (2017)
47. D.H. Kim, W.H. Park, H.G. Oh et al., Two-channel graphene pH sensor using semi-ionic fluorinated graphene reference electrode. *Sensors (Basel)* **20**(15), 4184 (2020)
48. T.Y. Kim, S.A. Hong, S. Yang, A solid-state thin-film Ag/AgCl reference electrode coated with graphene oxide and its use in a pH sensor. *Sensors (Basel)* **15**(3), 6469–6482 (2015)
49. Y.-R. Li, S.-H. Chang, W.-L. Tsai et al., Highly sensitive pH sensors of extended-gate field-effect transistor with the oxygen-functionalized reduced graphene oxide films on reverse pyramid substrates. *IEEE Electron Device Lett.* **36**(11), 1189–1191 (2015)
50. B. Maily-Giacchetti, A. Hsu, H. Wang et al., pH sensing properties of graphene solution-gated field-effect transistors. *J. Appl. Phys.* (2013). <https://doi.org/10.1063/1.4819219>
51. A. Medhat, D. Salah, N. Boichuk et al., Graphene nanoplatelet–Au nanoparticle hybrid as a capacitive-metal–oxide–semiconductor pH sensor. *ACS Appl. Electron. Mater.* **3**(1), 430–436 (2020)
52. S. Neupane, V. Subedi, K.K. Thapa et al., An alternative pH sensor: graphene oxide-based electrochemical sensor. *Emerg. Mater.* **5**(2), 509–517 (2021)
53. P. Salvo, N. Calisi, B. Melai et al., Temperature and pH sensors based on graphenic materials. *Biosens. Bioelectron.* **91**, 870–877 (2017)
54. W. Su, J. Xu, X. Ding, An electrochemical pH sensor based on the amino-functionalized graphene and polyaniline composite film. *IEEE Trans. Nanobiosci.* **15**(8), 812–819 (2016)
55. Z. Tehrani, S.P. Whelan, A.B. Mostert et al., Printable and flexible graphene pH sensors utilising thin film melanin for physiological applications. *2D Mater.* **7**(2), 024008 (2020)
56. F. Vivaldi, A. Bonini, B. Melai et al., A graphene-based pH sensor on paper for human plasma and seawater. *Annu. Int. Conf. IEEE Eng. Med. Biol. Soc.* **2019**, 1563–1566 (2019)
57. B. Wang, K.L. Liddell, J. Wang et al., Oxide-on-graphene field effect bio-ready sensors. *Nano Res.* **7**(9), 1263–1270 (2014)
58. Z.L. Wu, M.X. Gao, T.T. Wang et al., A general quantitative pH sensor developed with dicyandiamide N-doped high quantum yield graphene quantum dots. *Nanoscale* **6**(7), 3868–3874 (2014)
59. Y. Koval, Mechanism of etching and surface relief development of PMMA under low-energy ion bombardment. *J. Vac. Sci. Technol. B Microelectron. Nanometer Struct. Process. Meas. Phenom.* **22**(2), 843–851 (2004)

Springer Nature or its licensor (e.g. a society or other partner) holds exclusive rights to this article under a publishing agreement with the author(s) or other rightsholder(s); author self-archiving of the accepted manuscript version of this article is solely governed by the terms of such publishing agreement and applicable law.